CrossMark

Influence of Doping and Nanostructuration on n-Type $Bi_2(Te_{0.8}Se_{0.2})_3$ Alloys Synthesized by Arc Melting

Mouna Gharsallah[1,2], Federico Serrano-Sanchez[1], Norbert M. Nemes[1,3*], Jose Luis Martinez[1] and Jose Antonio Alonso[1]

Abstract

In competitive thermoelectric devices for energy conversion and generation, high-efficiency materials of both n-type and p-type are required. For this, Bi_2Te_3-based alloys have the best thermoelectric properties in room temperature applications. Partial replacement of tellurium by selenium is expected to introduce new donor states in the band gap, which would alter electrical conductivity and thermopower. We report on the preparation of n-type $Bi_2(Te_{1-x}Se_x)_3$ solid solutions by a straightforward arc-melting technique, yielding nanostructured polycrystalline pellets. X-ray and neutron powder diffraction was used to assess Se inclusion, also indicating that the interactions between quintuple layers constituting this material are weakened upon Se doping, while the covalency of intralayer bonds is augmented. Moreover, scanning electron microscopy shows large surfaces perpendicular to the c crystallographic axis assembled as stacked sheets. Grain boundaries related to this 2D nanostructuration affect the thermal conductivity reducing it below 0.8 $Wm^{-1}K^{-1}$ at room temperature. Furthermore, Se doping increases the absolute Seebeck coefficient up to -140 μV K^{-1} at 400 K, which is also beneficial for improved thermoelectric efficiency.

Keywords: Thermoelectrics, Nanostructuration, Lattice thermal conductivity, Bismuth telluride, Neutron powder diffraction

Background

In a sustainable-energy environment, the conversion between thermal and electrical energy carried out by thermoelectric materials has become essential. Thermoelectric devices present several advantages such as reliability, absence of mobile parts and durability. Such devices shall find a large spectrum of applications ranging from refrigeration to waste heat recovery, temperature measurements and thermal energy detection [1–6]. The performance of thermoelectric materials is evaluated by the figure of merit (ZT) defined as:

$$ZT = T\,S^2\sigma/\kappa$$

where T is the average absolute temperature, S is the Seebeck coefficient, σ is the electrical conductivity, and κ is the total thermal conductivity.

Thus, on the path towards more efficient thermoelectric materials, it is necessary to achieve the best compromise between these three intrinsic physical quantities S, σ, and κ. In thermoelectric research, this challenging task is broached through many different ways. Band engineering, hierarchical architectures, complex crystal structures, and rattling semiconductors are amongst recent approaches for ZT improvement [7–10]. Nanostructuration also plays an essential role, as there are many theoretical and experimental works showing enhanced thermoelectric efficiency in bulk nanostructured and nanosized materials, where the relevant physical properties may be decoupled [11–13].

Most thermoelectric materials are heavily doped narrow band-gap semiconductors where the concentration of charge carriers has been optimized to offer a high electric conductivity while maintaining elevated Seebeck coefficients and low electronic thermal

* Correspondence: nmnemes@fis.ucm.es
[1]Instituto de Ciencia de Materiales de Madrid, C.S.I.C., Cantoblanco, E-28049 Madrid, Spain
[3]Departamento de Física de Materiales, Universidad Complutense de Madrid, E-28040 Madrid, Spain
Full list of author information is available at the end of the article

Springer Open

Gharsallah *et al. Nanoscale Research Letters* (2017) 12:47

Page 2 of 8

conductivity. Bismuth chalcogenides and, in particular, Bi_2Te_3 and its solid solutions, are known as the most efficient thermoelectric materials for near room temperature applications [5, 14]. Their thermoelectric performance is notably affected by their exact stoichiometry, as Te and Bi vacancies and lattice (antisite) defects directly vary the carrier concentration.

Fine adjustment of the carrier concentration is done mainly by doping and controlling the synthesis conditions. Diverse methods are employed for the preparation of thermoelectric materials, from physical methods, such as high-energy ball milling, melting, and hot pressing, to wet chemical methods, such as polyol synthesis of nanoparticles [15]. Present in all these methods, after the prior preparation of the material, is a compaction step and/or steps of conditioning, comprising time-consuming processes, and expensive instrumentation.

Thermoelectric properties of bismuth telluride-related compounds are usually optimized by various technical processes, such as ionic and element substitution [16–18], changes in the intricate macro- and micro-structure [19–26] and diverse variations in the synthesis conditions [27–29]. The inclusion of Se in bismuth telluride-type compounds, constituting Bi_2Te_3-Bi_2Se_3 solid solutions, enlarges the band-gap energy by stronger Se-Bi interactions and creates new donor levels close to the bulk band gap, which may increase the electrical conductivity [30–32], thus enhancing the thermoelectric performance. Furthermore, doping-induced point defects, such as atomic mass fluctuation and lattice deformation, yield a reduction in the lattice thermal conductivity. Besides, nanostructured composites present low-energy electron filtering and enhanced phonon scattering [11, 33] at the interfaces, although a strong drawback has been found in Se-doped polycrystalline samples as this improvement is countered by deteriorating electrical conductivity. This effect is attributed to the higher sensitivity of n-type $Bi_2Te_{3-x}Se_x$ to the lattice directions than the parent compound and p-type $Bi_{2-x}Sb_xTe_3$, for which bulk samples commonly present randomly orientated grains; therefore, many efforts are still to be made to achieve bulk nanostructured samples with increased phonon scattering while keeping a preferential orientation to maintain the power factor (defined as the product of S^2 and σ) [34, 35].

Recently, we have reported on a direct method to synthesize highly nanostructured Bi_2Te_3 samples in short reaction times, in the form of robust pellets directly usable in devices [36]. The structural characterization showed a near-perfect stoichiometry and an important anisotropy of the atomic displacement factors. Electrical conductivity was notably improved while thermal conductivity was not enlarged. Based on these results, we prepared doped samples for the optimization of the thermoelectric parameters.

In this paper, we describe the preparation of n-type $Bi_2Te_{2.4}Se_{0.6}$ by the same straightforward arc-melting procedure. We found a huge preferred orientation and nanostructuration while a decrease in thermal and electrical conductivity is observed. The sample was structurally characterized by X-ray diffraction (XRD) and neutron powder diffraction (NPD), since neutrons provide a bulk analysis and avoid preferred orientation problems. A microscopic study of the nature of the raw material was realized by SEM, and the three thermoelectric properties (Seebeck, electrical, and thermal conductivity) were measured.

Methods

The n-type $Bi_2[Te_{0.8}Se_{0.2}]_3$ alloy was synthesized in an Edmund Buhler mini-arc furnace using direct arc melting in a water cooled copper crucible with a tungsten electrode under purified argon atmosphere. The starting materials were pure elements of Bi (99.999%, Cerac), Te (99.999%, Alfa Aesar), and Se (99.95%, Alfa Aesar) that were weighted and mixed according to the stoichiometric ratio. The mixed powders were put into pellets and molten and re-molten four times to promote homogenization. It was also necessary to work in a slight argon overpressure and to carry out several argon rinsing cycles in order to purify the atmosphere bell. In order to minimize the evaporation effects, we reduced the melting time and controlled the arc power supply to use the lowest current that melts the mixture. After melting, the ingot was ground to powder several times in an agate mortar previous to structural characterization.

Structural phase analysis was carried out using X-ray diffraction (XRD) by Cu Kα radiation on a Bruker-AXS D8 diffractometer (40 kV, 30 mA), run by DIFFACT^{PLUS} software, in Bragg-Brentano reflection geometry with Cu Kα radiation ($\lambda = 1.5418$ Å). The data were collected by 0.04 steps over a 2θ range from 10° to 64°.

The structure, phase purity, and homogeneity of the elaborated sample were checked by NPD. The crystallographic structure was refined from a high-resolution NPD pattern collected at the HRPT diffractometer of the SINQ neutron source at the Paul Scherer Institute in Villigen (Switzerland), with a wavelength $\lambda = 1.494$ Å. Cylindrical vanadium holders were used to pack the samples (diameter 8 mm), counting during 2 h in the high-intensity mode; the sample holder was rotating during the acquisition time. The diffraction data were analyzed by the Rietveld method using the FULLPROF program [37]. The line shape of the diffraction peaks was generated by a Thompson-Cox-Hastings pseudo-Voigt function. 8.532, 5.800, and 7.970 fm were, respectively, the coherent scattering lengths used for Bi, Te, and Se. A preferred orientation correction accounting for platelets perpendicular to [001] direction was added to the refinement. There were

Gharsallah *et al. Nanoscale Research Letters* (2017) 12:47

Page 3 of 8

no regions excluded in the refinement. In the final runs, the following parameters were refined: scale factor; background coefficients; zero-point error; pseudo-Voigt corrected for asymmetry parameters; occupancy of Bi, Te, and Se; positional coordinates; and anisotropic displacements for all the atoms. Superficial analysis by FE-SEM was performed in a FEI-Nova microscope.

Measurements of thermoelectric transport properties were carried out in a commercial system (physical property measurement system (PPMS) by Quantum Design). The measurements were made in the residual vacuum of He atmosphere, under a pressure of 10^{-5} Torr, in the

temperature range of 2 to 400 K. Disks of 10 mm diameter, featuring perfectly parallel faces, were obtained by treatment of the as-grown ingots under an isostatic pressure of 10^3 psi. These disks where then cut with a diamond saw to bar-shaped specimens. The size of the n-$Bi_2Te_{2.4}Se_{0.6}$ pellets were typically $10 \times 3 \times 1.5$ mm^3 with four Cu wires attached with EPO-TEK® H20E paste. Thermoelectric properties were measured perpendicular to the pellet pressing direction. Throughout the whole temperature range, a temperature gradient of 3% was used.

The Hall coefficient was measured using the resistivity option of the PPMS system in an approximate van der
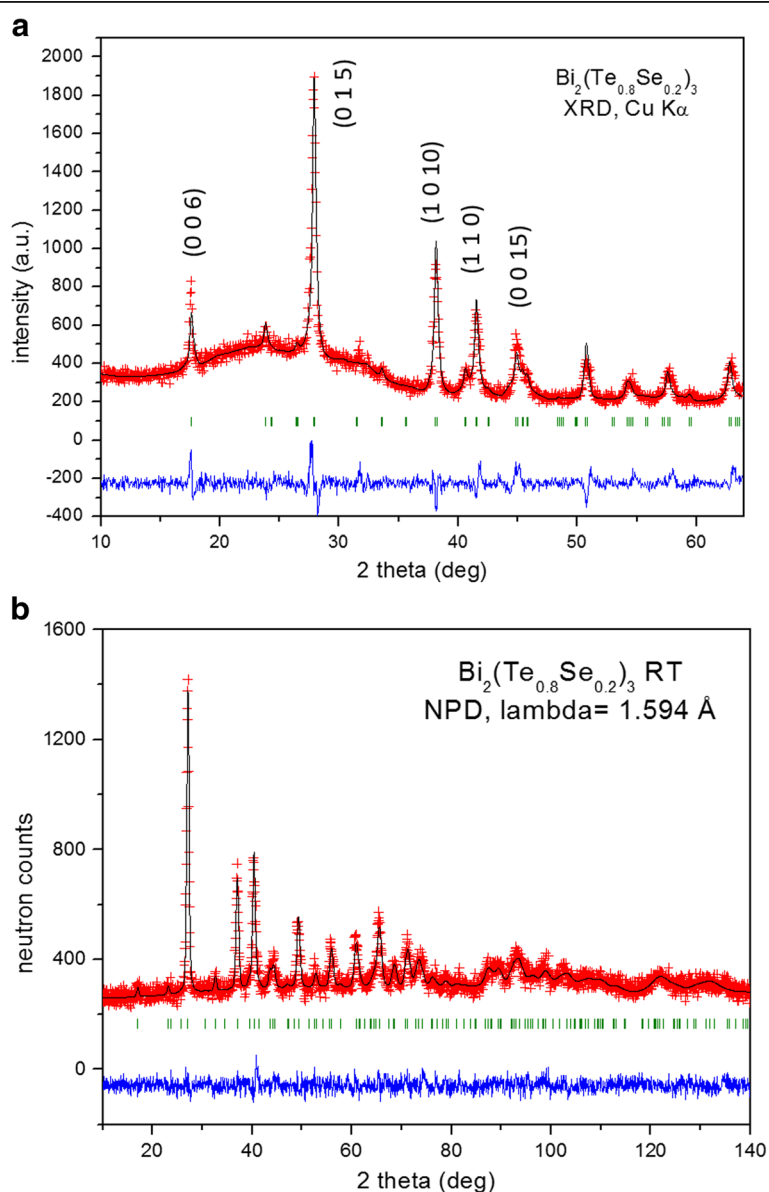

Fig. 1 a Pattern from XRD data for ground n-$Bi_2Te_{2.4}Se_{0.6}$, showing refinement by the Rietveld method in the space group R-3m. There is a notable preferred orientation, increasing the [001] reflections. **b** Calculated (*full line*), difference (*at the bottom*), and observed (*crosses*) neutron powder diffraction patterns for n-$Bi_2Te_{2.4}Se_{0.6}$ at 298 K

Gharsallah *et al. Nanoscale Research Letters* (2017) 12:47

Page 4 of 8

Pauw geometry, in the disk-shaped pellets with spring-loaded pins for contacts. The charge carrier concentration was determined via the relation $n = -1/R_H e^-$ from the Hall coefficient R_H.

Results and discussion

Crystal structure

A representative Rietveld refinement of the XRD pattern for n-type $Bi_2Te_{2.4}Se_{0.6}$ (Fig. 1a) shows a Bi_2Te_3-type structure, defined in the space group R-3m. Patterns show a strong preferred orientation enhancing the (0 0 *l*) reflections, pointing to a strongly textured as-grown sample. In order to improve the match between observed and simulated profiles, a preferred orientation function was introduced as correction during the profile refinement.

Crystallographic analysis by neutron powder diffraction (NPD) allows investigating the essential structural details of $Bi_2Te_{2.4}Se_{0.6}$, including the anisotropic displacement factors. Preferred orientation effects are largely eliminated by the measurement conditions: neutrons can penetrate bulk amounts of material, which are ground to powder, packed into vanadium cylinders that are furthermore rotating continuously during data collection. Also, the lack of form factor in neutron diffraction means that high-angle diffraction peaks are also well resolved, which allows determining precisely the anisotropic displacement factors. Refinement of NPD data at RT of the crystal structure was carried out in the Bi_2Te_3-type model [38] defined in the hexagonal setting of the rhombohedral R-3m space group (no. 12), $Z = 3$, with Bi located at 6c (0 0 z) Wyckoff site and the two types of tellurium and selenium, Te1/Se1 at 3a (0 0 0) positions and Te2/Se2 at 6c. Calculated profiles present an excellent agreement with the experimental data (Fig. 1b). A minor preferred orientation correction effectively improved the refinement for all the reflections. Table 1 presents the main atomic parameters, displacements factors, and discrepancy factors resulting from the refinement. Unit-cell parameters are $a = 4.3315$ (4) and $c = 30.208$ (5) Å. Unit-cell size is significantly reduced from that of the parent Bi_2Te_3 compound (with unit-cell parameters: $a = 4.385915$ (6), $c = 30.495497$ (1) Å, [35]), which can be understood as a consequence of the smaller ionic size of Se^{2-} vs Te^{2-}.
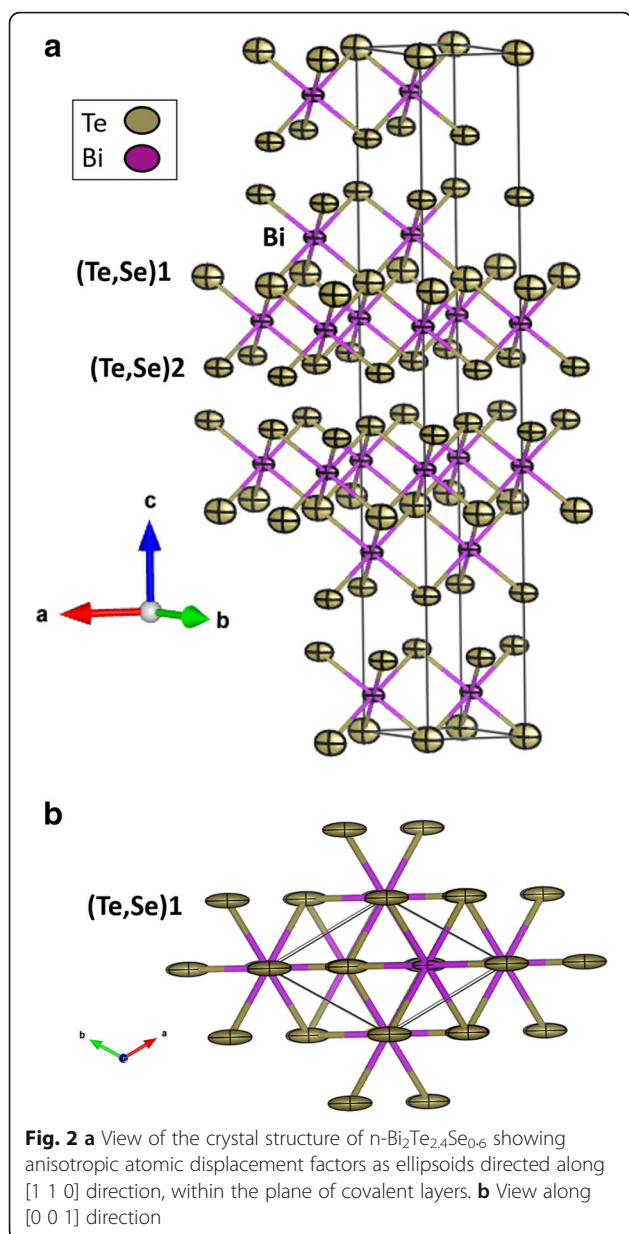
Figure 2 shows two views of the crystal structure of $Bi_2Te_{2.4}Se_{0.6}$. Similar to Bi_2Te_3, it is made up of hexagonal close-packed sheets of a series of quintuple layers with a stacking sequence of covalently bonded A2-Bi-A1-Bi-A2 atoms (A = Te or Se), as shown in Fig. 2a. The interlayer forces between quintuple layers (A2-A2 interactions) are principally weak van der Waals type. Therefore, crystals of these compounds are easily cleaved parallel to ab plane. Interestingly, Se atoms were found, by the NPD Rietveld refinement, to be randomly distributed at both Te sublattices. This is somewhat contrary to expectations, as there is a

Table 1 Structural parameters for $Bi_2(Te_{0.8}Se_{0.2})_3$ refined in the R-3m space group (hexagonal setting) from NPD data collected at RT. The discrepancy factors after the refinement are also included

Fractional atomic coordinates and equivalent isotropic displacement parameters

	Wyckoff site	x	y	z	U_{eq}	Occ. (<1)
Bi	6c	0.00000	0.00000	0.3956 (4)	0.009 (4)	
Te1	3a	0.00000	0.00000	0.00000	0.025 (11)	0.80 (9)
Se1	3a	0.00000	0.00000	0.00000	0.025 (11)	0.20 (9)
Te2	6c	0.00000	0.00000	0.7897 (3)	0.017 (8)	0.79 (3)
Se2	6c	0.00000	0.00000	0.7897 (3)	0.017 (8)	0.21 (3)

Anisotropic displacement parameters ($Å^2$)

	U^{11}	U^{22}	U^{33}	U^{12}	U^{13}	U^{23}
Bi	0.009 (2)	0.009 (2)	0.009 (8)	−0.005 (2)	0.00000	0.00000
Te1	0.020 (7)	0.020 (7)	0.04 (2)	−0.010 (7)	0.00000	0.00000
Se1	0.020 (7)	0.020 (7)	0.04 (2)	−0.010 (7)	0.00000	0.00000
Te2	0.016 (5)	0.016 (5)	0.019 (12)	−0.008 (5)	0.00000	0.00000
Se2	0.016 (5)	0.016 (5)	0.019 (12)	−0.008 (5)	0.00000	0.00000

Discrepancy factors

$R_p = 2.69\%$, $R_{wp} = 5.89\%$, $R_{exp} = 5.36\%$, $\chi^2 = 1.21$, $R_{Bragg} = 5.15\%$

Unit-cell parameters: $a = 4.3315$ (4) Å and $c = 30.208$ (5) Å, $V = 490.9$ (1) $Å^3$, $Z = 3$

slight difference in the chemical environment of Te1 and Te2 which gives Bi-Te1 bond a minor ionic component, favoring that Se would first preferentially replace Te2 sites [39], immediately followed by random introduction of Se at Te1 sites. Terminal Te2/Se2 atoms are covalently bonded to three Bi atoms at 3.050 (9) Å, with the non-bonding electron pairs directed to the interlayer spacing, while Te1/Se1 is coordinated to six Bi atoms in octahedral sites at distances of 3.161 (7) Å. Bi is coordinated to 3 Te1/Se1 plus 3 Te2/Se2 forming a distorted octahedron. Additionally, the analysis of the neutron data yielded accurate anisotropic displacement factors for all the atoms. Figure 2b, in particular, shows the elongated ellipsoids of (Te, Se)1 directed along the cell diagonal [1 1 0] direction. The refinement of the occupancy factors of Bi, Se, and Te stoichiometry is obtained with standard deviations (±0.02). One of the strengths of this study, using NPD, is that we can give a bulk characterization of any possible off-stoichiometry. The stoichiometry change due to evaporation loss of the elements is thus evaluated by NPD, refining the occupation factor of each atom position. Despite the possible evaporation of the various elements during arc melting, NPD shows practically the same ratio as the weighed elements before the synthesis, in our process.
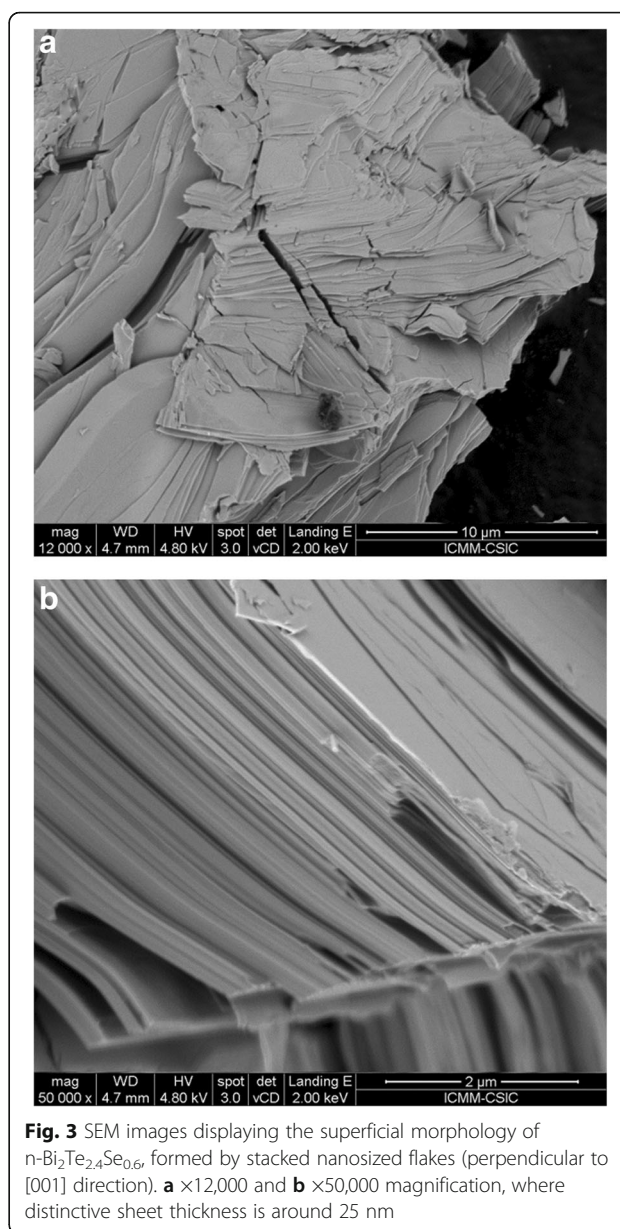
It is interesting to compare these results with similar structural refinements recently published for pristine Bi_2Te_3 [36]. We observe that both Bi-Te1 distances (3.253 Å) and Bi-Te2 distances (3.061 Å) decrease upon

Gharsallah *et al. Nanoscale Research Letters* (2017) 12:47

Page 5 of 8

Fig. 2 a View of the crystal structure of n-$Bi_2Te_{2.4}Se_{0.6}$ showing anisotropic atomic displacement factors as ellipsoids directed along [1 1 0] direction, within the plane of covalent layers. **b** View along [0 0 1] direction

Fig. 3 SEM images displaying the superficial morphology of n-$Bi_2Te_{2.4}Se_{0.6}$, formed by stacked nanosized flakes (perpendicular to [001] direction). **a** ×12,000 and **b** ×50,000 magnification, where distinctive sheet thickness is around 25 nm

Se introduction, which is an additional indication that Se doping occurs at both un-equivalent positions. Regarding the connections established between the quintets, of van der Waals type (Te_2/Se_2-Te_2/Se_2), the distance is 3.691 (9) Å vs 3.660 (6) Å calculated for pristine Bi_2Te_3 from the data of reference [36]; the increase in covalency within the quintuple layers seems to imply a decrease of the inter-layer interactions, with a significant separation of adjacent covalent blocks.
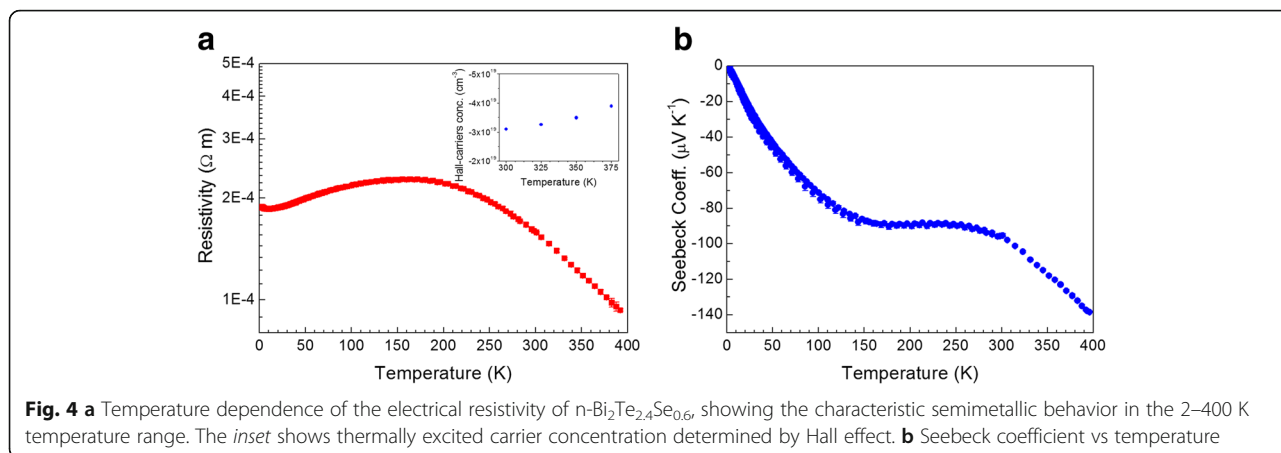
Nanostructuration

Figure 3a, b displays the superficial morphology of the as-grown $Bi_2Te_{2.4}Se_{0.6}$ pellets collected with increasing magnification (×12,000 and ×50,000, respectively) in SEM. The sample is formed of stacked nanosized sheets, each of them apparently single crystalline, with the large surfaces perpendicular to the *c* crystallographic axis. The characteristic cleavage of this material is apparent, a consequence of weak bonding between quintuple layers. The typical thickness of individual sheets is around 25 nm. The low thermal conductivity of this material produced by arc melting is probably related to this nanostructuration into separate sheets providing many surface boundaries, which increases phonon scattering.

Transport measurements

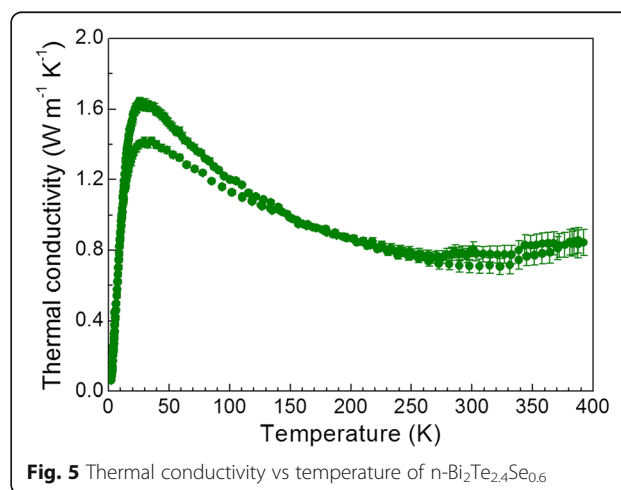The temperature-dependent electrical resistivity is shown in Fig. 4a. The sample shows semimetallic behavior in the

Gharsallah *et al. Nanoscale Research Letters* (2017) 12:47

Page 6 of 8

Fig. 4 a Temperature dependence of the electrical resistivity of n-Bi$_2$Te$_{2.4}$Se$_{0.6}$, showing the characteristic semimetallic behavior in the 2–400 K temperature range. The *inset* shows thermally excited carrier concentration determined by Hall effect. **b** Seebeck coefficient vs temperature

sense that its resistivity at low temperatures increases with temperature, as for a metal, but at higher temperatures it decreases, as for a semiconductor, until reaching a minimum measured value of 100 μΩ m at 365 K. For arc-melted Bi$_2$Te$_3$, resistivity values as low as 2 μΩ m are found at 320 K [36], while for samples prepared by other physical and wet chemical methods, resistivity values are around 30 and 5 μΩ m [40]. Therefore, in Se-doped Bi$_2$Te$_3$ arc melting leads to high electrical resistivity, even though for the undoped compound we obtained an improvement in the electrical conductivity [36]. These results are related to the scattering of carriers in grain boundaries and the point defects introduced by the random distribution of Te and Se in the crystalline positions. Soni et al. [39] found similar effects on carrier scattering, doping, and electrical conductivity for a Bi$_2$Te$_{2.2}$Se$_{0.8}$ nanocomposite, with both metallic and semiconductor behavior throughout their measurement range with values around 75 μΩ at room temperature. By encapsulating melting and hot pressing, this value is reduced down to 12–20 μΩ m [41], while after SPS treatments, values close to 15 μΩ m were reported [35].

The n-type Hall-carrier concentration (inset of Fig. 4a) increases with increasing temperature due to thermal excitation, typical of semiconducting behavior. We find the charge carrier density at 300 K to be −3.1·10^{19} cm^{-3}, slightly higher than pure Bi$_2$Te$_3$ [36, 42]. The mobility is quite low at 300 K, determined using $\mu_H = R_H * \sigma$, which results in 10.1 cm^2 V^{-1} s^{-1} [35, 41]. Bi$_2$Te$_3$-type compounds are extremely anisotropic, where electron mobility is heavily influenced by the grain orientation [43].

The Seebeck coefficient vs temperature is shown in Fig. 4b. The n-type Seebeck coefficient progressively increases between 2 and 400 K, reaching −140 μV K^{-1} at 390 K. The plateau in the Seebeck coefficient is related to the maximum found in the electrical resistivity. We can think of two effects that may explain this behavior: Thermal excitation of carriers diminishes bipolar

transport at higher temperatures, causing a shift of the temperature dependence of the Seebeck coefficient, too. Also, potential barrier scattering, a thermally activated process that increases the Seebeck coefficient, may play an important role in the highly granular material produced by arc melting [44]. These results were checked in numerous samples. In comparison, the parent compound Bi$_2$Te$_3$ shows similar n-type semimetallic behavior, with reported values in the range of −50 to −260 μV K^{-1} for samples prepared by different chemical and physical methods [15, 42, 45]. In particular, arc melting yields samples with around −50 μV/K [36]. For Se-doped samples, similar Seebeck coefficients at 300 K close to −150 μV K^{-1} are reported [41]; much better values are reported by Soni et al. [39] after tuning the Se composition, where the optimal thermoelectric performance has been found in Bi$_2$Te$_{2.7}$Se$_{0.3}$ nanocomposite, which exhibits its best Seebeck coefficient value of −259 μV/K at room temperature.

Figure 5 displays the evolution of total thermal conductivity vs temperature. At low temperature, it shows the expected Umklapp maximum and then it decreases

Fig. 5 Thermal conductivity vs temperature of n-Bi$_2$Te$_{2.4}$Se$_{0.6}$

Gharsallah *et al. Nanoscale Research Letters* (2017) 12:47

Page 7 of 8

throughout the measurement range to a minimum value of 0.8 W m^{-1} K^{-1} at room temperature. This is one of the best (lowest) values for the Bi$_2$Te$_3$ system [15], typically above 0.9 W m^{-1} K^{-1}. This value is lower than that obtained in our previous study for nanostructured Bi$_2$Te$_3$ obtained by arc melting, where thermal conductivity reached 1.2 W m^{-1} K^{-1} at 365 K [36]. This reduction could be related to the higher anisotropy and electrical resistivity, nanostructuration, and point defects induced by Se doping. The underlying reason is likely the strong phonon scattering at grain boundaries associated with the sheet-type nanostructuration. For the nanostructured parent compound Bi$_2$Te$_3$ prepared by ball milling and hot pressing, measured thermal conductivities were 1.2 W m^{-1} K^{-1} at 330 K [46], and for chemically prepared samples, the thermal conductivity values are around 0.8 W m^{-1} K^{-1} at 380 K [45].

Within the Bi$_2$Te$_3$-Bi$_2$Se$_3$ system, for solid solutions prepared by encapsulated melting and hot pressing, typical thermal conductivity values of 1.04 W m^{-1} K^{-1} at 323 K have been reported [41]; for samples prepared by large-scale zone melting κ = 1.2 W m^{-1} K^{-1} at 323 K [44]. In the case of nanocomposite materials prepared by the polyol method and SPS, much lower values of thermal conductivity are found such as 0.9 W m^{-1} K^{-1} at 300 K for Bi$_2$Te$_{2.2}$Se$_{0.8}$ nanocomposites and exceptionally 0.7 W m^{-1} K^{-1} at 300 K for Bi$_2$Te$_{2.7}$Se$_{0.3}$ nanocomposites [39], but these fabrication techniques are, by far, more complex and time-consuming than the arc melting presented here.

Conclusions

A Se-doped Bi$_2$Te$_3$ specimen of composition Bi$_2$Te$_{2.4}$Se$_{0.6}$ has been synthesized by a straightforward arc-melting technique, yielding highly nanostructured samples in short reaction times, with improved thermal transport properties. A structural NPD study yields interesting hints on the increased covalency of the quintuple layers and the weakening of the interactions between adjacent layers upon Se doping. As a consequence of this structural feature, the trend to cleave and to form nanostructured specimens increases with respect to the pristine Bi$_2$Te$_3$ alloy. The Se doping (located at both Te1 and Te2 crystallographic sites, as shown from NPD data) enhances the carrier scattering, thus diminishing the electrical conductivity and results in low mobility. The Bi$_2$(Te$_{1-x}$Se$_x$)$_3$ system is notably affected by the nanostructuration which leads to improved (lower) thermal conductivities.

Abbreviations
2D: Two dimensional; FE-SEM: Field effect scanning electron microscope; HRPT: High-resolution powder diffractometer for thermal neutrons; NPD: Neutron powder diffraction; PPMS: Physical property measurement system; PSI: Paul Scherrer Institute; R$_H$: Hall coefficient; RT: Room temperature; *S*: Seebeck coefficient; SEM: Scanning electron microscopy; SINQ: The Swiss spallation neutron source; SPS: Spark plasma sintering; *T*: Temperature; XRD: X-ray diffraction; ZT: Thermoelectric figure of merit; κ: Thermal conductivity; μ_H: Hall mobility; σ: Electric conductivity

Authors' contributions
MG synthesized the samples. FSS and NNM carried out the transport experiments. FSS and JAA performed the structural characterization work. JLM, NNM, and JAA conceived of the study. All authors participated in discussing the results and commented on the manuscript. All authors read and approved the final manuscript.

Competing interests
The authors declare that they have no competing interests.

Ethics approval and consent to participate
No ethical issues are raised by this research concerning patient participation or personal data.

Author details
^{1}Instituto de Ciencia de Materiales de Madrid, C.S.I.C., Cantoblanco, E-28049 Madrid, Spain. ^{2}Sfax University, National School of Engineers, Sfax BPW 3038, Tunisia. ^{3}Departamento de Física de Materiales, Universidad Complutense de Madrid, E-28040 Madrid, Spain.

References
1. DiSalvo F (1999) Thermoelectric cooling and power generation. Science (80-) 285:703–706. doi:10.1126/science.285.5428.703
2. Sales B (2002) Smaller is cooler. Science (80-) 295:1248–1249. doi:10.1126/science.1069895
3. Riffat SB, Ma X (2003) Thermoelectrics: a review of present and potential applications. Appl Therm Eng 23:913–935. doi:10.1016/S1359-4311(03)00012-7
4. Bell LE (2008) Cooling, heating, generating power, and recovering waste heat with thermoelectric systems. Science 321:1457–1461. doi:10.1126/science.1158899
5. Snyder GJ, Toberer ES (2008) Complex thermoelectric materials. Nat Mater 7:105–114. doi:10.1038/nmat2090
6. Martín-González M, Caballero-Calero O, Díaz-Chao P (2013) Nanoengineering thermoelectrics for 21st century: energy harvesting and other trends in the field. Renew Sustain Energy Rev 24:288–305. doi:10.1016/j.rser.2013.03.008
7. Slack GA, Tsoukala VG (1994) Some properties of semiconducting IrSb3. J Appl Phys 76:1665–1671. doi:10.1063/1.357750
8. Chen G, Dresselhaus MS, Dresselhaus G et al (2003) Recent developments in thermoelectric materials. Int Mater Rev 48:45–66. doi:10.1179/095066003225010182
9. Bilc DI, Hautier G, Waroquiers D et al (2015) Low-dimensional transport and large thermoelectric power factors in bulk semiconductors by band engineering of highly directional electronic states. Phys Rev Lett 114:1–5. doi:10.1103/PhysRevLett.114.136601
10. Wang Y, Huang H, Ruan X (2014) Decomposition of coherent and incoherent phonon conduction in superlattices and random multilayers. Phys Rev B 90:48–50. doi:10.1103/PhysRevB.90.165406
11. Dresselhaus MS, Chen G, Tang MY et al (2007) New directions for low-dimensional thermoelectric materials. Adv Mater 19:1043–1053. doi:10.1002/adma.200600527
12. Peranio N, Eibl O, Bäßler S et al (2015) From thermoelectric bulk to nanomaterials: current progress for Bi 2 Te 3 and CoSb 3. Phys Status Solidi A 11:1–11. doi:10.1002/pssa.201532614
13. Kanatzidis MG (2010) Nanostructured thermoelectrics: the new paradigm? Chem Mater 22:648–659. doi:10.1021/cm902195j

Gharsallah *et al. Nanoscale Research Letters* (2017) 12:47

Page 8 of 8

14. Boyer A, Cissé E (1992) Properties of thin film thermoelectric materials: application to sensors using the Seebeck effect. Mater Sci Eng B 13:103–111. doi:10.1016/0921-5107(92)90149-4

15. Lan Y, Minnich AJ, Chen G, Ren Z (2010) Enhancement of thermoelectric figure-of-merit by a bulk nanostructuring approach. Adv Funct Mater 20: 357–376. doi:10.1002/adfm.200901512

16. Chung D-Y, Hogan T, Brazis P et al (2000) CsBi 4 Te 6 : a high-performance thermoelectric material for low-temperature applications. Science (80-) 287: 1024–2027. doi:10.1126/science.287.5455.1024

17. Polvani DA, Meng JF, Chandra Shekar NV et al (2001) Large improvement in thermoelectric properties in pressure-tuned p-type Sb 1.5 Bi 0.5 Te 3. Chem Mater 13:2068–2071. doi:10.1021/cm000888q

18. Lukyanova LN, Kutasov VA, Konstantinov PP, Popov VV (2010) Improved thermoelectrics based on bismuth and antimony chalcogenides for temperatures below 240 K. Adv Sci Technol 74:77–82. doi:10.4028/www. scientific.net/AST.74.77

19. Venkatasubramanian R, Siivola E, Colpitts T, O'Quinn B (2001) Thin-film thermoelectric devices with high room-temperature figures of merit. Nature 413:597–602. doi:10.1038/35098012

20. Singh MP, Bhandari CM (2003) Thermoelectric properties of bismuth telluride quantum wires. Solid State Commun 127:649–654. doi:10.1016/ S0038-1098(03)00520-9

21. Zhao XB, Ji XH, Zhang YH et al (2005) Bismuth telluride nanotubes and the effects on the thermoelectric properties of nanotube-containing nanocomposites. Appl Phys Lett 86:062111. doi:10.1063/1.1863440

22. Zhou J, Jin C, Seol JH et al (2005) Thermoelectric properties of individual electrodeposited bismuth telluride nanowires. Appl Phys Lett 87:1–3. doi:10.1063/1.2058217

23. Lee S, Von Allmen P (2006) Tight-binding modeling of thermoelectric properties of bismuth telluride. Appl Phys Lett 88:1–3. doi:10.1063/1.2162863

24. Bulman GE, Siivola E, Shen B, Venkatasubramanian R (2006) Large external DeltaT and cooling power densities in thin-film Bi 2Te3-superlattice thermoelectric cooling devices. Appl Phys Lett. doi:10.1063/1.2353805

25. Yang B, Han ZH (2006) Temperature-dependent thermal conductivity of nanorod-based nanofluids. Appl Phys Lett 89:083111. doi:10.1063/1.2338424

26. Ni HL, Zhao XB, Zhu TJ et al (2005) Synthesis and thermoelectric properties of Bi2Te3 based nanocomposites. J Alloys Compd 397:317–321. doi:10.1016/ j.jallcom.2005.01.046

27. Yamashita O, Tomiyoshi S, Makita K (2003) Bismuth telluride compounds with high thermoelectric figures of merit. J Appl Phys 93: 368–374. doi:10.1063/1.1525400

28. Walachová J, Zeipl R, Zelinka J et al (2005) High room-temperature figure of merit of thin layers prepared by laser ablation from Bi2Te3 target. Appl Phys Lett 87:3–6. doi:10.1063/1.2001755

29. Su T, Zhu P, Ma H et al (2006) Electrical transport and high thermoelectric properties of PbTe doped with Bi2Te3 prepared by HPHT. Solid State Commun 138:580–584. doi:10.1016/j.ssc.2006.04.018

30. Yan X, Poudel B, Ma Y et al (2010) Experimental studies on anisotropic thermoelectric properties and structures of n-type Bi2Te2.7Se0.3. Nano Lett 10:3373–3378. doi:10.1021/nl101156v

31. Scheele M, Oeschler N, Veremchuk I et al (2010) ZT enhancement in solution-grown Sb(2-x)BixTe 3 nanoplatelets. ACS Nano 4:4283–4291. doi:10.1021/nn1008963

32. Nolas GS, Sharp J, Goldsmid HJ (2001) Thermoelectrics: basic principles and new materials developments

33. Medlin DL, Snyder GJ (2009) Interfaces in bulk thermoelectric materials. A review for current opinion in colloid and interface science. Curr Opin Colloid Interface Sci 14:226–235. doi:10.1016/j.cocis.2009.05.001

34. Ryu B, Kim B-S, Lee JE et al (2016) Prediction of the band structures of Bi2Te3-related binary and Sb/Se-doped ternary thermoelectric materials. J Korean Phys Soc 68:115–120. doi:10.3938/jkps.68.115

35. Choi S-M, Lee KH, Lim YS et al (2016) Effects of doping on the positional uniformity of the thermoelectric properties of n-type Bi2Te2.7Se0.3 polycrystalline bulks. J Korean Phys Soc 68:17–21. doi:10.3938/jkps.68.17

36. Gharsallah M, Serrano-Sánchez F, Bermúdez J et al (2016) Nanostructured Bi 2 Te 3 Prepared by a Straightforward Arc-Melting Method. Nanoscale Res Lett 11:142. doi:10.1186/s11671-016-1345-5

37. Rodríguez-Carvajal J (1993) Recent advances in magnetic structure determination by neutron powder diffraction. Phys B 192:55–69, doi: http://dx.doi.org/10.1016/0921-4526(93)90108-l

38. Adam A (2007) Rietveld refinement of the semiconducting system Bi2 −xFexTe3 from X-ray powder diffraction. Mater Res Bull 42:1986–1994. doi:10.1016/j.materresbull.2007.02.027

39. Ajay S, Zhao Y, Yu L, Michael Khor Khiam A, Mildred S, Dresselhaus QX (2012) Enhanced thermoelectric properties of solution grown Bi2Te3−xSex nanoplatelet composites. Nano Lett 12:1203–1209, dx.doi.org/10.1021/nl2034859

40. Zhao LD, Zhang B-P, Liu WS et al (2009) Effects of annealing on electrical properties of n-type Bi2Te3 fabricated by mechanical alloying and spark plasma sintering. J Alloys Compd 467:91–97. doi:10.1016/j.jallcom.2007.12.063

41. Lee G-E, Eum A-Y, Song K-M et al (2015) Preparation and thermoelectric properties of n-type Bi2Te2.7Se0.3:D m. J Electron Mater 44:1579–1584. doi: 10.1007/s11664-014-3485-7

42. Feng S-K, Li S-M, Fu H-Z (2014) Probing the thermoelectric transport properties of n-type Bi 2 Te 3 close to the limit of constitutional undercooling. Chinese Phys B 23:117202. doi:10.1088/1674-1056/23/11/117202

43. Ohsugi IJ, Kojima T, Sakata M et al (1994) Evaluation of anisotropic thermoelectricity of sintered Bi 2Te3 on the basis of the orientation distribution of crystallites. J Appl Phys 76:2235–2239. doi:10.1063/1.357641

44. Wang S, Li H, Lu R et al (2013) Metal nanoparticle decorated n-type Bi2Te3-based materials with enhanced thermoelectric performances. Nanotechnology 24:285702. doi:10.1088/0957-4484/24/28/285702

45. Saleemi M, Toprak MS, Li S et al (2012) Synthesis, processing, and thermoelectric properties of bulk nanostructured bismuth telluride (Bi 2 Te 3). J Mater Chem 22:725–730. doi:10.1039/C1JM13880D

46. Yang JY, Fan XA, Chen RG et al (2006) Consolidation and thermoelectric properties of n-type bismuth telluride based materials by mechanical alloying and hot pressing. J Alloys Compd 416:270–273. doi:10.1016/j. jallcom.2005.08.054